Environmental Modelling & Software 24 (2009) 436–443

Contents lists available at ScienceDirect

Environmental Modelling & Software

journal homepage: www.elsevier.com/locate/envsoft

Comparison of land surface temperature (LST) modeled with a spatially-distributed solar radiation model (SRAD) and remote sensing data

Jingfen Sheng*, John P. Wilson, Sujin Lee

Department of Geography, University of Southern California, Los Angeles, CA 90089-0255, USA

ARTICLE INFO

Article history:
Received 12 July 2007
Received in revised form 3 September 2008
Accepted 14 September 2008

Keywords:
Spatially distributed solar radiation model
Land surface temperature
Remote sensing data

ABSTRACT

The solar radiation model SRAD was applied to a Mediterranean mountainous environment in southern California for estimating land surface temperature (LST). The simulated SRAD LST results were compared with high- and meso-resolution satellite-based LST data at daily, monthly and annual temporal scales to identify potential ways of improving the LST accuracy in either the SRAD or satellite-based approaches. It was found that mean monthly and annual LST from SRAD closely matched the MODIS LST observations (but for the fact they were from 0.7 to 1.5 °C lower) while the daily LST from SRAD agreed less well with ASTER observations and were 2.1 °C and 4.8 °C higher for 01/23/05 and 07/21/06, respectively. High mountainous, steep and south/north facing slopes resulted in large discrepancies in LST estimates and the winter LST estimates are more sensitive to terrain factors and their associated land use/cover characteristics than the summer estimates. It is therefore suggested that vertically variable elevation lapse rates, spatially distributed surface albedo and leaf area index for the time-specific simulations that represent the heterogeneity of land surface characteristics be used in SRAD inputs. The results also show how instantaneous model outputs rather than lumped average daily outputs offer better comparisons with satellite based data as well.

1. Introduction

Understanding dynamic watershed hydrologic processes requires fine spatial and temporal resolution models coupled to extensive databases of surface flow and groundwater. However, acquiring fine-scale hydrologic parameters over large geographic extents is logistically problematic and presently not possible. Observations in topographically rugged terrain are especially rare. Many GIS models and/or hydrologic simulations therefore have been developed over the past decades to quantify the spatial and temporal distribution of selected hydrologic components like precipitation, evapotranspiration, infiltration, water storage and runoff - see, for example, various solar radiation models (e.g. r.sun, Krcho, 1990; Scharmer and Greif, 2000; SolarFlux, Dubayah and Rich, 1995; Solar Analyst, Fu and Rich, 2000; and SRAD, Wilson and Gallant, 2000b), and rainfall-runoff models (e.g. TR-55, NRCS, 1986; MIKE-SHE, DHI, 1993; CASC2D, Julien et al., 1995; HEC-HMC, USACE-HEC, 1998; SWMM, EPA, 2000; and F2D, Skahill and Johnson, 2000).

In environmental modeling one model or instrument can rarely provide all of the optimum datasets that are needed to describe the relationships associated with atmosphere, hydrology or land surfaces. For any particular phenomenon there are potentially many non-overlapping different explanations and/or models that can be formulated (Richardson, 2003). This state of affairs therefore inevitably leads to the assessment of the level of uncertainty associated with different models and/or data and the need to identify the 'effective' model and datasets and the conditions at which models operate. This is an issue of increasing importance in hydrologic modeling as the traditional hydrologic models are supplemented with more and more remotely sensed and GIS-based model derived datasets. Limited by sparse and relatively rare in situ observation data and the complexity of land surface processes, relatively little is known about the quality of those models/data at varying scales and contexts (Schoorl et al., 2000) such that it is difficult to test whether one or more of these models is capable of providing accurate estimates of hydrologic parameters for various projects.

With this in mind, the results of an experimental multi-scale study of land surface temperature estimation (LST) are presented in this article. Land surface temperature is one of the key environmental variables required to drive hydrologic models and characterize a wide variety of energy fluxes as well as water budgets (Mannstein, 1987; Sellers et al., 1988; Davis, 1998; Park et al., 2005). More importantly, accurate estimation of LST from existing models and satellite data is still a challenging task in various disciplines of

* Corresponding author. Tel.: +1 213 821 1313.
E-mail addresses: sheng@usc.edu (J. Sheng), jpwilson@usc.edu (J.P. Wilson), sujinlee@usc.edu (S. Lee).

1364-8152/$ – see front matter © 2008 Elsevier Ltd. All rights reserved.
doi:10.1016/j.envsoft.2008.09.003

remote sensing, atmospheric science, hydrology, etc. The comparative results presented in this article aim to identify potential ways of improving LST accuracy in either the SRAD or satellite-based approaches. So the overarching goals of this study are two-fold. The first is the estimation of LST using the SRAD model and satellite-based data for a small semi-arid study area. The second is to compare the SRAD LST estimates at different temporal scales with the satellite-based LST data and test the sensitivity of LST in different seasons and various topographic settings.

The SRAD model, as described by Wilson and Gallant (2000b), is a spatially distributed solar radiation model for predicting a complex set of short- and long-wave solar energy fluxes at and near the earth's surface. The model calculates potential solar radiation as a function of latitude, elevation, slope, aspect, topographic shading, and time of year, and then modifies this estimate using information about monthly average cloudiness and sunshine fraction. SRAD also estimates the LST at each grid point as a function of the mean monthly average surface temperature, the minimum, maximum and average temperature lapse rates, and elevation for a reference climatic station (as specified in the site-parameter file). Temperature is extrapolated across the surface using a method based on Running et al. (1987), Hungerford et al. (1989), Running (1991), and Running and Thornton (1996) that corrects for elevation via a lapse rate, slope-aspect via a short-wave radiation ratio, and vegetation effects via a leaf area index. This approach means that the topographic effects of slope, aspect, and shading on radiation as well as land surface temperature are calculated by SRAD.

Although based on a simplified representation of the underlying physics, the main solar radiation factors are considered and the model is able to characterize the spatial variability of the landscape processes at the topo- and meso-scales. The model has previously been run for only a few locations in Australia (e.g. Moore et al., 1993; Loughhead, 1994; Mullen, 1995), one mountainous region in the western United States (Wilson and Gallant, 2000b) and in a boreal forest environment in the northwestern portion of the province of Ontario, Canada (McKenney et al., 1999). McKenney et al. (1999) calibrated and tested SRAD estimates of annual solar radiation with irradiance data as measured at nearby radiation stations (i.e. stations within 580–900 km of their study area), estimated from interpolated radiation surfaces, and from a published map of national radiation isolines. The SRAD estimates were found to be consistent with irradiance data from other sources, but the test was limited due to the lack of in situ spatially distributed observations and was inadequate to specify the spatial and temporal accuracy of SRAD over different landscapes and various temporal scales in estimating solar radiation and other land surface parameters such as land surface temperature.

Remotely sensed observations from satellites provide accurate information about land surface properties that are useful for validating, and therefore improving global meteorological model predictions after appropriate aggregation and parameterization (Price, 1982; Diak and Whipple, 1993). But satellite-based LST are not ground truthed and subject to the uncertainties embedded in the various algorithms. The two LST data sources used in this study for comparison are collected from two sensors onboard NASA's TERRA satellite, the Earth Observing System Moderate Resolution Imaging Spectroradiometer (MODIS) and the Advanced Spaceborne Thermal Emission and Reflection Radiometer (ASTER). ASTER and MODIS provide consistent LST data with a potentially better accuracy than 1 °C from −10 °C to 50 °C at a global scale (Hook and Prata, 2001; Wan et al., 2002, 2004; Jacob et al., 2004). Wan et al. (2002) showed that the MODIS LST agreed with in situ measured LST within +/− 1 K in the range 263–322 K for six sites in Railroad Valley and one site with snowcover in Bridgeport, CA. The retrieved LST data were also recommended for use in bare and sparsely vegetated areas. More importantly, ASTER is set up to acquire high spatial resolution 90 m LST, which therefore effectively captures the spatial variation of LST in response to heterogeneous land surface processes (Abrams et al., 2002). MODIS, on the other hand, collects data at a moderate spatial resolution (i.e. 1 km) with almost daily coverage of the Earth (Justice et al., 1998). Therefore, the ASTER and MODIS satellites together provide relatively fine spatial resolution and multi-temporal remotely sensed datasets that can be used to parameterize the key inputs to various environmental models.

However, these high resolution satellite-based LST data are certainly not accurate in every circumstance and for every land use and land cover type. In particular, it is known that land surface elements including thermal properties retrieved from satellites lose accuracy in areas with high relief due to the assumption of horizontal homogeneity made in various atmospheric correction algorithms (Dubayah, 1992; Wang et al., 2005). The error caused by not considering terrain complexity is considerable when the sun elevation is relatively low or the terrain is relatively complex even when the resolution is greater than 1 km (as is achieved with the so-called moderate or low resolution satellites) (Dubayah, 1992; Wang et al., 2005). Land use and land cover also influence surface emissivity and lead to the uncertainty in LST estimation particularly in semi-arid and arid regions (Wan et al., 2002). The complexity of land surface types and sensor performance limit the accuracy of satellite LST measurement such that the operation and utilization of the data was restrained in regional climate prediction (Sun et al., 2004). Some studies have also clearly suggested the necessity of confirmation of the MODIS global 1 °C accuracy for LST for a range of cover types (Snyder et al., 1997). The validation of remotely sensed LST using ground-based measurements alone confronts difficulties because of large spatial variations in the in situ LST measurement data and the influences of spatial variability in atmosphere absorption and earth surface emissivity (Schmugge and Schmidt, 1998; Wan et al., 2002; Yang and Yang, 2006). So cross-validation of the satellite retrieved LST with other sources of observed or modeled LST may provide useful insights for improving algorithm accuracy. The SRAD model used in this study can possibly compensate for the topographic corrections in the satellite-based LST and therefore provide enhanced LST retrieval algorithms in both instances.

In the following sections, we set out to summarize briefly the SRAD, ASTER, and MODIS LST generation, compare the SRAD estimates with the MODIS and ASTER observations at the daily, monthly and annual scales, investigate the spatial and temporal discrepancies in LST estimates between SRAD and ASTER/MODIS, and finally test seasonal and topographic effects on LST estimation in order to identify potential ways to improve the model performance.

2. Methods

2.1. The study area

The analyses were based on datasets from a small part of the San Fernando Valley area centered at 34.26°N 118.19°W in Los Angeles County, California (Fig. 1). The study area was defined by a 783 × 602 square grid DEM with a 30 m resolution to satisfy the processing capacity of SRAD. It sat along the southern foothills of the San Gabriel Mountains with 85% of the land surface covered by trees, grasses, and shrubs (e.g. sagebrush, chaparral, and woodland), and the final 15% by urban land uses. The elevation ranged from 158 to 1875 m above sea level with an average slope of 18%. In the dry season, eastern Pacific high pressure dominates the weather in Los Angeles. A marine layer is produced as warm and very dry air descending from this Pacific high caps cool, ocean-modified air under a strong inversion, The marine layer is a prominent feature of the weather in the Los Angeles Basin from late spring through early fall (NOAA, 2006). The wet season that typically runs from November through April is dominated by the northern hemisphere polar jet stream. Pacific storms, sometimes fed with subtropical moisture, often push cold fronts across California from northwest to southeast. These storms and frontal systems account for the bulk of the area's annual rainfall (NOAA, 2006).

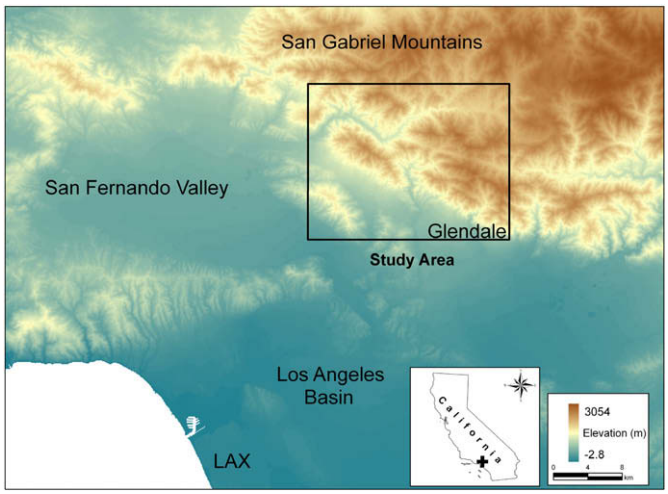

Fig. 1. Study area and adjacent region.

2.2. Experimental design

In order to examine the LST discrepancies occurring at different times and scales, a total of 32 LST surfaces were produced or compiled from SRAD and the ASTER/MODIS products. The DEM and input parameter file were processed multiple times by SRAD to produce LST surfaces for a single day (01/23/05, 07/21/06), individual months (01/05 and 01/06 through 12/06), and an entire year (2006). The two LST surfaces for 01/23/05 and 01/05 were selected to represent the winter LST distribution for the comparison with the summer LST estimates and variations with terrain factors. ASTER provided two daily LST surfaces for 01/23/05 and 07/21/06 when the least cloud coverage was present. MODIS provided monthly LST products for 01/05, and 01/06 through 12/06, and one annual LST surface for 2006. The monthly SRAD LST surfaces estimated for 2006 and corresponding 8-day MOD11A2 products were used to examine the seasonal effects on LST.

The LST estimates from SRAD were plotted against the LST values obtained from the ASTER/MODIS products at corresponding locations and times to examine the overall correlations and the variation over different times and scales on a pixel-by-pixel basis. The mean absolute error (MAE) surfaces between the SRAD and ASTER/MODIS LST estimates were also analyzed to see the correlation between the MAE and the underlying topographic attributes and the land cover/land use properties. The MAE surfaces were derived by subtracting the MODIS LST surface from the corresponding SRAD LST surfaces and MAE were summarized using Zonal Statistics in ArcGIS Spatial Analyst 9.2.

Biases in monthly mean, minimum and maximum SRAD and MODIS estimates were analyzed to examine the seasonal effects on LST estimates. The effects of elevation, slope and aspect on the SRAD LST estimates and ASTER/MODIS LST measurements were examined using Zonal Statistics in ArcGIS Spatial Analyst 9.2 as well. The elevation surface was classified into five intervals: <400 m, 400–700 m, 700–1000 m, 1000–1300 m, and >1300 m. The slope and aspect surfaces were generated from a 30 m DEM. The slope surface was classified into four slope classes, namely, flat lands (0–15%), gentle slopes (15–30%), moderate slopes (30–45%) and steep slopes (>45%). The aspect surface was classified into 45° classes representing N, NE, E, SE, S, SW, W, and NW slopes. LST statistics were calculated for each elevation range, slope and aspect class in ArcGIS Spatial Analyst 9.2.

2.3. Building the SRAD LST surfaces

The minimum air, maximum air, and surface temperatures, T, at each grid point were computed using:

$$T = T_b - \frac{T_{lapse}(z - z_b)}{1000} + C\left(S - \frac{1}{s}\right)\left(1 - \frac{LAI}{LAI_{max}}\right) \quad (1)$$

where z is the elevation of the grid point, z_b is the elevation of the temperature reference station, T_b is the temperature at the reference station (monthly minimum air, maximum air, or surface), T_{lapse} is the monthly temperature lapse rate (°C/1000), C is a constant (currently set to 1.0), s is the short wave radiation ratio at each grid point, which equals the ratio of the daily total or global short-wave irradiance on horizontal and sloping sites, respectively, LAI is the leaf area index at the grid cell, and LAI_{max} is the maximum leaf area index. A complete description on how solar radiation is calculated in SRAD is provided by Wilson and Gallant (2000b).

SRAD requires the user to specify the number of time steps, the period of calculation, an input DEM, and a parameter file. The input parameter file is of great importance and composed of a series of 15 local monthly radiation, temperature, and vegetation parameters which SRAD uses to calculate incident and outgoing irradiance fluxes, as well as surface and air temperatures for each point in the DEM. Those parameters were compiled from solar radiation and meteorological data derived from local meteorological stations and MODIS products as listed in Table 1. Table 2 presents the full set of parameters that were used in the SRAD model. It is important to note here that parameter files for the daily LST estimate were compiled in ways such that the radiation pattern and weather condition on that day were matched, which also means that parameters such as sunshine fraction, land surface temperature, air temperature were set to match the particular daily values observed on ASTER or MODIS images rather than the mean monthly values used for monthly and annual estimates. The surface temperature lapse rates were derived from satellite LST data since no ground measurements were available for the study area. Interestingly, the lapse rate for 01/23/05 based on ASTER data was as low as 0.3 °C/km, which fell outside the ranges for this parameter recommended by Wilson and Gallant (2000b). Therefore, the average monthly surface temperature lapse rate of 6.5 °C/km was used for that particular SRAD run.

2.4. Compiling the ASTER/MODIS LST data

The MODIS and ASTER LST products represent the kinetic temperature determined by the thermal infrared (TIR) radiation from the surfaces of all of the components within the grid cells, including the vegetation, soil, water bodies (if any), and whatever else is observed by the satellite instruments. The overpass time of the satellite nadir observations is around 10:30 a.m. local solar time in the daytime and around 10:30 p.m. local solar time at night. The land surface observations are made around the overpass time on a global daily basis. The daily 90 m resolution ASTER Surface Kinetic Temperature (AST_08) for the study area for 01/23/05 and 07/21/06 was obtained from the EOS-Land Processes Distributed Active Archive Center (LP DAAC) to evaluate the daily LST generated by SRAD. The daily 1 km resolution level-3 MOD11A1 LST product, available from EDC DAAC (http://edcdaac.usgs.gov/modis/dataprod.html), was retrieved with the generalized split-window algorithm (Wan and Dozier, 1996) from the calibrated radiance data in bands 31 and 32. Eight consecutive daily MOD11A1 products were further averaged into 8-day products (MOD11A2). Detailed descriptions of the science data sets included in the MODIS LST products of MOD11A1 and MOD11A2 are given at http://edcdaac.usgs.gov/modis/dataproducts.asp#mod11.

The monthly daytime LST surfaces were constructed simply by averaging three consecutive MOD11A2 products. The 8-day MOD11A2 products with cloud

Table 1
SRAD input parameters and data sources.

Parameters	Data sources
Sunshine fraction	Number of hours of daily sunshine (n) obtained from National Climatic Data Center (NCDC) at http://www.ncdc.noaa.gov/oa/ncdc.html (Los Angeles International Airport; 33.93°N 118.38°W) Theoretical N derived using the method of Allen et al. (1998)
Cloudiness	Total irradiation obtained from California Irrigation Management Information System (CIMIS) at http://wwwcimis.water.ca.gov/cimis/data.jsp (Glendale 34.2°N 118.23°W) Clear-sky total irradiation estimated using the method of Wilson and Gallant (2000b)
Atmospheric transmittance at sea level	Extraterrestrial irradiance
Circumsolar coefficient	Direct irradiance obtained from the National Solar Radiation Data Base (NSRDB) at http://rredc.nrel.gov/solar/old_data/nsrdb/
Albedo	Land cover data obtained from California Department of Forest and Fire Protection (CDFFP) CALVEG database at http://frap.cdf.ca.gov/data/frapgisdata/select.asp Monthly albedo for each type of vegetation obtained from Terjung et al., (1969)
LAI	Monthly LAI derived from MOD15A2 for each month. The spatially distributed monthly LAI values were averaged over the entire study area to obtain a single mean LAI value for each month
Surface emissivity	Monthly mean values derived from MOD11C3 Band31/band32
Land surface temperature	Monthly mean values derived from MOD11A2 products. Daily LST were derived from ASTER
Air temperature	Daily and monthly temperature derived from CIMIS at Glendale
Lapse rate	Specified lapse rates were estimated on a daily/monthly basis by identifying pairs of low-elevation/high-elevation stations at Glendale and Mt Wilson

Table 2
SRAD input parameters for generating daily, monthly and annual LST surfaces.

Lines	23-Jan	Feb	Mar	Apr	May	Jun	21-Jul	Aug	Sep	Oct	Nov	Dec
1	34.17	34.33										
2	0.13	0.15	0.16	0.20	0.22	0.23	0.21	0.19	0.16	0.15	0.14	0.12
3	0.2	0.2	0.17	0.17	0.16	0.16	0.16	0.16	0.16	0.16	1.17	0.2
4	0.24	0.24	0.24	0.17	0.27	0.28	0.11	0.04	0.21	0.21	0.24	0.23
5	1	0.71	0.71	0.79	0.64	0.62	1	0.85	0.75	0.75	0.7	0.73
6	24.3	17.6	19.2	19.8	22.8	24.5	34.6	29.1	27.7	24.0	20.7	18.4
7	10	6.1	7.1	7.9	11.0	12.9	18.2	15.2	14.4	11.4	8.0	6.1
8	26.0	19.2	22.5	29.7	34.0	40.8	51.5	37.5	26.4	26.9	19.0	15.5
9	6.5	10.6	9.0	7.8	11.3	10.9	9.6	7.5	10.0	7.0	6.6	6.7
10	9.8	2.6	7.6	6.8	0.5	−2.5	−3.5	−3.6	−1.0	5.3	1.7	3.6
11	11.8	7.0	8.0	6.5	−0.9	0.0	1.5	0.5	1.5	6.1	4.4	6.6
12	1											
13	2.17	2.3	1.4	2.9	3.7	3.5	3	2.8	2.5	2.3	2	2.1
14	10	0.98	0.00008	338.7								
15	0.61	0.59	0.63	0.57	0.66	0.67	0.61	0.64	0.67	0.64	0.65	0.57
	Jan-05	Feb	Mar	Apr	May	Jun	Jul-06	Aug	Sep	Oct	Nov	Dec
5	0.7	0.71	0.71	0.79	0.64	0.62	0.92	0.85	0.75	0.75	0.7	0.73
6	17.6	20.2	15.2	18.1	22.6	28.0	31.6	28.5	28.2	23.4	23.1	19.2
7	7.2	5.7	4.8	7.8	11.7	14.1	16.8	13.8	14.2	11.1	8.9	5.8
8	19.0	19.2	22.5	29.7	34.0	40.8	37.8	37.5	26.4	26.9	19.0	15.5
9	6.5	10.3	8.6	7.0	10.6	10.0	8.9	6.6	9.2	6.7	6.3	6.6
10	9.8	2.6	7.6	6.8	0.5	−2.5	−3.5	−3.6	−1.0	5.3	1.7	3.6
11	11.8	7.0	8.0	6.5	−0.9	0.0	1.5	0.5	1.5	6.1	4.4	6.6
	Jan-06	Feb-06	Mar-06	Apr-06	May-06	Jun-06	Jul-06	Aug-06	Sep-06	Oct-06	Nov-06	Dec-06
5	0.7	0.69	0.72	0.73	0.75	0.8	0.92	0.92	0.89	0.82	0.8	0.74
6	18.5	20.2	15.2	18.1	22.6	28.0	31.6	28.5	28.2	23.4	23.1	19.2
7	6.2	5.7	4.8	7.8	11.7	14.1	16.8	13.8	14.2	11.1	8.9	5.8
8	17.0	19.2	22.5	29.7	34.0	40.8	37.8	37.5	26.4	26.9	19.0	15.5
9	6.5	10.3	8.6	7.0	10.6	10.0	8.9	6.6	9.2	6.7	6.3	6.6
10	4.7	2.6	7.6	6.8	0.5	−2.5	−3.5	−3.6	−1.0	5.3	1.7	3.6
11	6.1	7.0	8.0	6.5	−0.9	0.0	1.5	0.5	1.5	6.1	4.4	6.6

Other lines are not changed.
Line 1, latitude min/max; line 2, circumsolar coefficient for each month; line 3, albedo; line 4, alpha cloudiness parameter; line 5, sunshine fraction; line 6, average max air temperature C from CIMIS Glendale Station; line 7, average min air temperature C from CIMIS Glendale Station; line 8, average surface temperature C from ASTER/MODIS at the Glendale Station; line 9, the elevation lapse rate of average surface temperature derived from the corresponding ASTER/MODIS LST data and DEM.; line 10, the elevation lapse rate of min air temperature derived from the climate stations located within the study area between the Glendale and Mt Wilson stations.; line 11, the elevation lapse rate of max air temperature derived from the climate stations located within the study area between the Glendale and Mt Wilson stations.; line 12, NLAI, the number of leaf area index (LAI) profiles; line 13, LAI from MODIS 2006; line 14, Four miscellaneous parameters: the maximum leaf area index; ES, the surface emissivity; TRANCO, the elevation lapse rate of atmospheric transmissivity—typically 0.00008; RELEV, the elevation of the temperature reference station (m). Line 15, atmospheric transmittance from MODIS 2006.

contamination were excluded from the monthly average LST calculations because of missing values in the cloud covered areas. This approach meant that 42 of 44 selected MOD11A2 granules were included (those captured on 03/31/06 and 07/21/06 were dropped) in our study area. The annual daytime LST surface was then obtained by averaging the monthly LST surfaces.

All MODIS and ASTER data were in the HDF-EOS format and were converted to geographical compatible formats (i.e. GeoTIFFs) using the HEG tool (see http://eosweb.larc.nasa.gov/PRODOCS/misr/tools/geotiff_tool.html). All the downloaded granules were projected to the Universal Transverse Mercator Projection (UTM) using the North American Datum of 1983 (NAD83) so that the satellite-image data matched the SRAD-generated LST estimates. No georectification was necessary for the satellite images and SRAD-generated surfaces in our case because the image data were released with geometric, radiometric and atmospheric corrections and registration with ground points.

3. Results

3.1. Comparisons of SRAD and ASTER/MODIS LST estimates at three temporal scales

Ten LST surfaces produced from SRAD and ASTER/MODIS at daily, monthly and annual scales are shown in Fig. 2. The median, minimum, maximum, first and third quartile values for these ten surfaces are plotted in Fig. 3. The daily LST estimates were 2.1 °C and 4.8 °C higher than the corresponding ASTER values for 01/23/05 and 07/21/06, respectively. Statistically significant differences were found between the mean LST values for the January, July and 2006 pairs with the SRAD LST values running from 0.7 to 1.3 °C lower than the corresponding satellite derived LST values. The very low values of LST from ASTER for 07/21/06 and MODIS for 07/06 were due to cloud contamination and were excluded from the pixel-by-pixel regression analysis that follows.

Fig. 4 shows the correlation between the SRAD and ASTER/MODIS estimates on a pixel-by-pixel basis at three time scales. The best coefficient of determination (R^2) was found for 2006 as a whole ($R^2 = 0.74$), compared to R^2 values of 0.01 and 0.38 for 01/23/05 and 07/21/06, respectively. The regression correlation was improved for 01/05, 07/06 and 2006 as the R^2 values got progressively larger with the estimates changing from daily to monthly and annual time periods.

3.2. Seasonal effects on LST estimates

There were significant trends in monthly mean LST biases with elevation by season (Fig. 5). Positive y values indicate that SRAD overestimated monthly LST while negative y values indicate that SRAD underestimated LST. Mean LSTs for February, March, May and June were closely reproduced by SRAD with reference to the MODIS mean values with differences of only 0.1 °C in February and March. But larger differences were found for the late summer, fall and winter: the mean monthly SRAD estimates were 1.1– 3.2 °C lower than the corresponding MODIS values during these periods. The consistency of the seasonal bias pattern in LST shows some agreement with the solar radiation modeling results obtained by Thornton et al. (2000) in Austria and the USA.

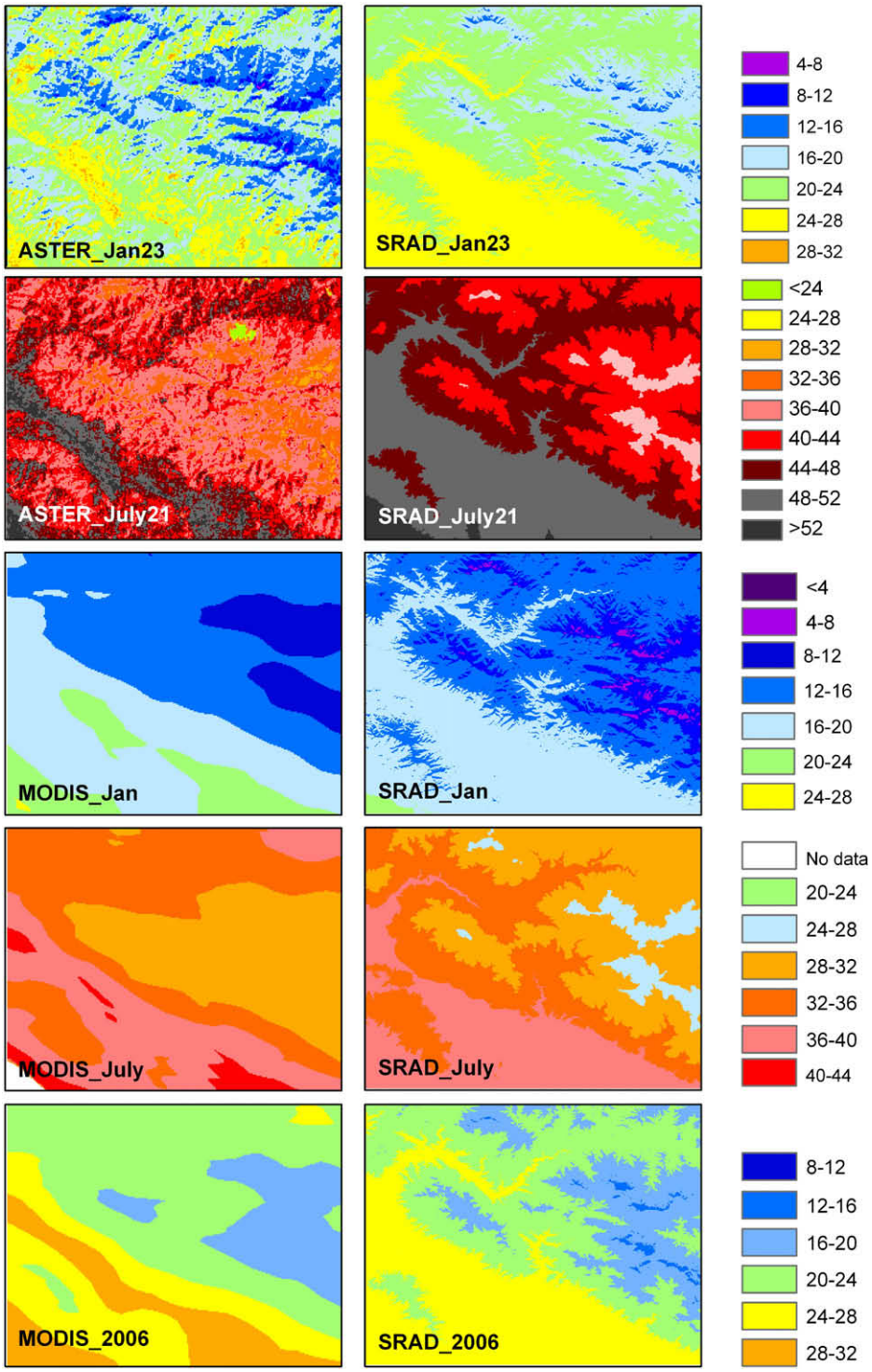

Fig. 2. LST surfaces generated by SRAD, ASTER/MODIS at daily, monthly and yearly scales.

3.3. *Influence of terrain on LST estimates*

The variation of LST with terrain factors of elevation, slope and aspect is shown in Fig. 6. The decrease in LST with increase in elevation was captured by SRAD and ASTER/MODIS (Fig. 6a). However, slight variations in the rates of decrease with increasing elevation were observed in ASTER/MODIS in contrast to SRAD for which the rates do not change across terrains and time scales. The rates derived from satellite LST values tend to be smaller at higher elevations and slightly larger on low elevation areas. The same issue of variable environmental temperature lapse rates was also raised by Thornton et al. (1997), who postulated that the environmental temperature lapse rate was usually greater for maximum temperature than for minimum temperature, resulting in smaller values of temperature differences at higher elevations. It is also found that slightly larger MAE values were associated with the high elevation class for the 2006 annual comparison. Larger MAE values were observed at both high and low elevation for the 07/06 summer

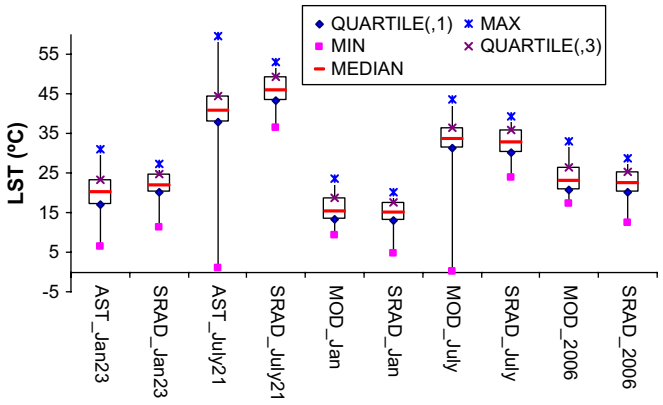

Fig. 3. Comparisons of basic statistics derived from generated LST surfaces.

comparison while small variations in MAE with elevation were observed for the 01/05 winter estimates. For the 07/21/06 daily LST estimates, the largest MAE values occurred at lower elevations and smaller MAE values were reported on the high mountain sites (Fig. 7a). MAE for 01/23/05 did not vary much with changing elevations.

Regardless of the temporal scale, mean LST values associated with flat slopes are significantly higher than other terrain positions (Fig. 6b). Minor variations were observed as slope increased. The percent error showed no consistent trend as slope changed at three temporal scales. The MAE values were exaggerated for the two winter dates on steeper slopes suggesting that winter LST values are more impacted by steep slopes. But interestingly, the largest MAE for 07/06 occurred on the flat slopes and became smaller as the slope became steeper (Fig. 7b).

In comparison, LST estimates vary more with aspect than slope. The south-facing slopes received the highest LST values and decreased consistently as aspect changed from south to north (Fig. 6c). The LST variation with aspect is larger in winter than summer (as would be expected give the latitude of the study area). The 01/23/05 LST estimated from SRAD was lower than the ASTER estimates on E-, SE-, and S- facing slopes while higher on W-, NW-, and N-facing slopes as a result of the uneven distribution of direct irradiation and vegetation cover with different aspects. This observation agrees with the findings by Kang et al. (2002) that the radiation derived from a topographic-based model was underestimated on south-facing slopes and over-estimated for north-facing slopes. In terms of the estimation bias, less bias in daily estimates occurred on south- compared to north-facing

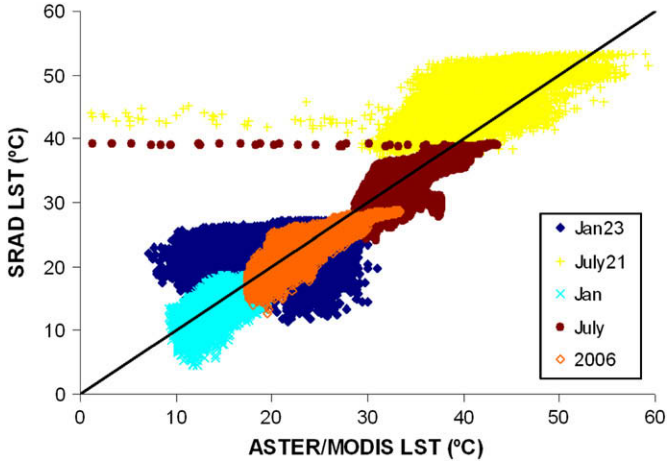

Fig. 4. Daily, monthly and yearly SRAD LST estimates plotted against ASTER/MODIS LST data. The solid line is the 1:1 line indicating no difference.

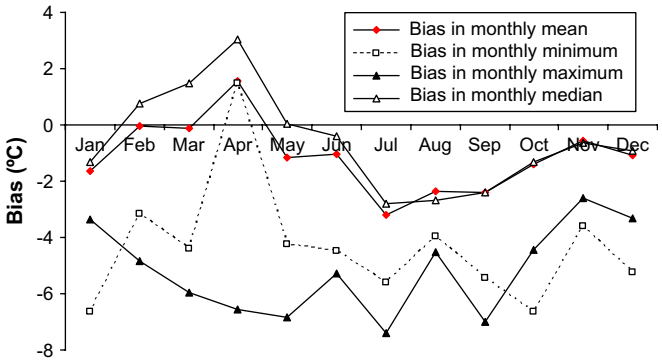

Fig. 5. Seasonal biases between monthly SRAD LST estimates and MODIS retrieved LST.

slopes. North-facing slopes produced larger MAE values during the winter simulations. This effect was reduced as the scale changed from daily to annual as demonstrated by the reduction in the variance in MAE from 0.7 to 0.1 for 01/23/05 and 2006, respectively (Fig. 7c). The sensitivity of LST estimates to terrain attributes indicates that high mountainous, steep and south/north facing slopes resulted in larger discrepancies in the LST estimates generated with the SRAD algorithms and satellite-based retrieval algorithms.

4. Discussion and conclusions

Discrepancies of various magnitudes were found between the satellite-based and SRAD LST values at different temporal scales. The difference can be attributed to the various factors and algorithms included in both approaches. This discussion will mainly focus on the potential ways of refining and improving SRAD.

First, the temporal granularity used to produce the two sets of estimates might have produced some systematic differences. The daily SRAD estimates were calculated at 12 min intervals and averaged from sunrise to sunset, while the retrieved LST surfaces were instantaneous measurements corresponding to the flight of the instruments (10:30 a.m. local solar time). During this study better daily LST estimates were achieved by matching the input parameters with the radiation pattern and weather conditions on the days of the simulations. Technically, this meant that parameters such as sunshine fraction, land surface temperature, and air temperature were set to match the particular daily values observed on the ASTER or MODIS images instead of using mean monthly values for the study area. This suggests that better results can be achieved by incorporating timely inputs in the SRAD parameter file to match the exact conditions of the date when the satellite overpasses or simulations are performed. Such functionality in SRAD output particularly matters when the estimations are made on a daily basis. The substantial differences between the SRAD estimates and ASTER observations observed for both daily comparisons are possibly due to the different time frames of the SRAD output and ASTER satellite observations. Further work is needed to modify SRAD so that it can produce (output) a series of instantaneous LST scenarios rather than the lumped average daily outputs used for this comparison. This modification of SRAD would improve the land surface property parameterization and extend the applicability of the TAPES and SRAD (Wilson and Gallant, 2000a) modeling frameworks.

Second, seasonal variations of LST differences observed between the satellite observations and SRAD estimates offer very interesting insights into refining both the SRAD and satellite algorithms. Using the monthly lumped input parameters, SRAD provided similar LST estimates for February, March, May and June but very different estimates for July through January. Further research is needed to explain their differences and assign causality to either SRAD and/or

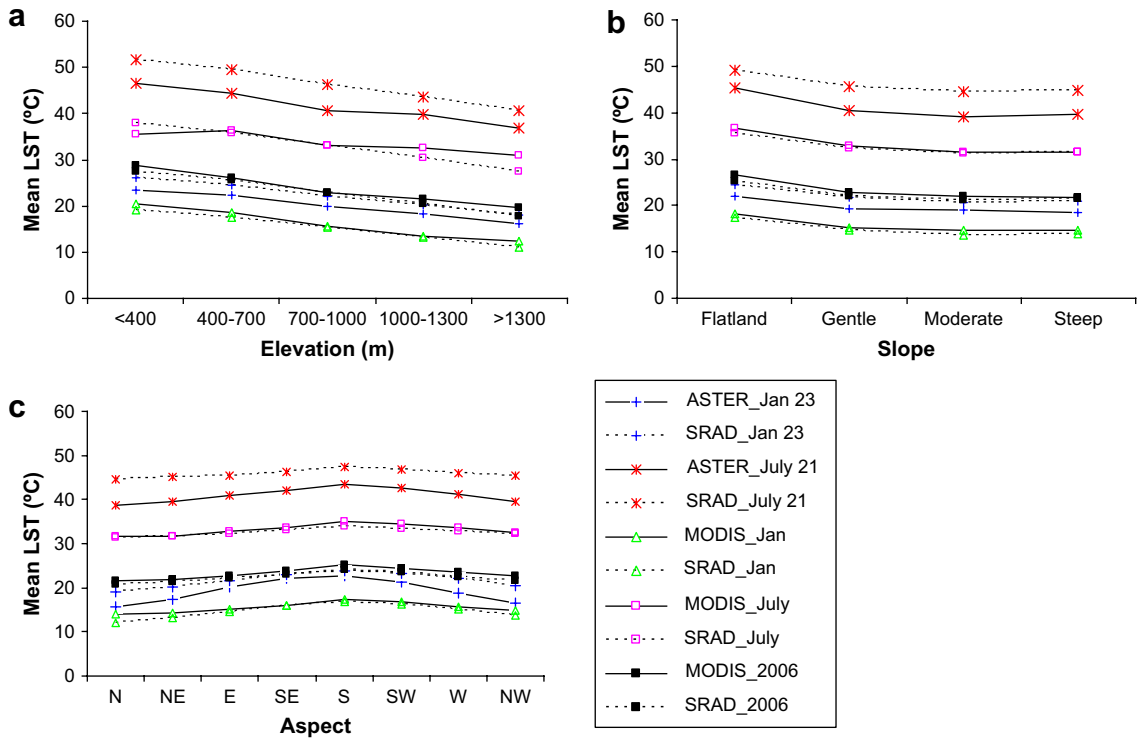

Fig. 6. Effects of (a) elevation; (b) slope; and (c) aspect on LST estimates.

the ASTER/MODIS algorithms. One possible explanation is that seasonal trends in temperature overlaid on the radiation-driven changes in diurnal temperature range lead to increased temperature lapse rates in the spring when temperatures are rising and decreased temperature lapse rates in the late summer, fall and winter as temperatures drop.

The discrepancies in daily, monthly and annual LST estimates between SRAD and ASTER/MODIS varied with topography and land use/land cover. High mountainous, steep and south/north facing slopes resulted in larger discrepancies in LST estimates. This result suggests it may be possible to apply potential corrections due to topographic and land surface effects in the ASTER/MODIS LST

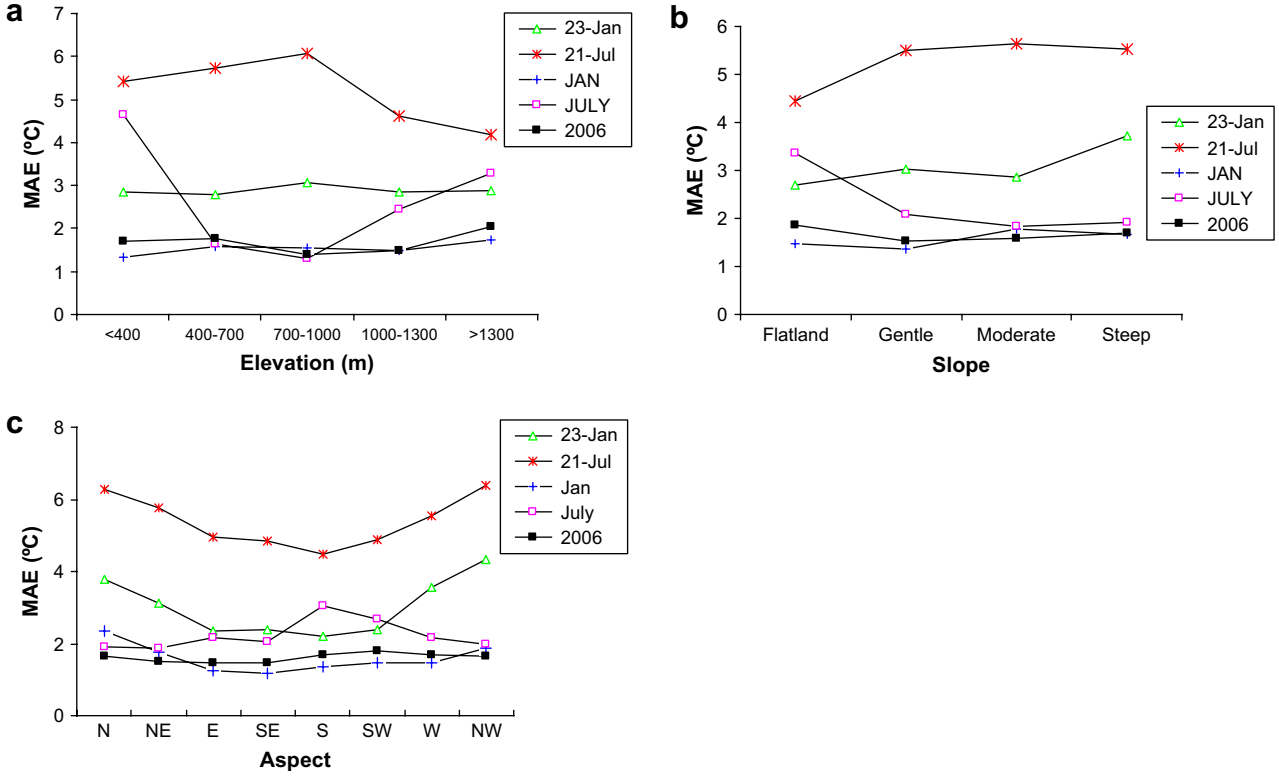

Fig. 7. Effects of (a) elevation; (b) slope; and (c) aspect on LST MAE.

retrieval algorithms by referring to the topographic components in SRAD. This finding confirmed the concerns noted earlier in the article that the satellite-based LST data lose accuracy in high relief areas and the results are sensitive to variations in emissivity in semi-arid and arid regions. Vertically variable temperature lapse rates that represent the heterogeneity of land surface characteristics could also be integrated in the SRAD algorithm to overcome the fixed rate approach that may have caused the discrepancies in LST estimates between SRAD and ASTER/MODIS.

To conclude the SRAD model was able to reproduce the satellite-based LST pattern and magnitude with various levels of success at different temporal scales. The mean monthly and annual LST from SRAD closely matched the MODIS LST observations (with differences ranging from 0.7 to 1.5 °C) and slightly larger differences of 2.1 °C and 4.8 °C reported for the daily SRAD LST and ASTER observations on 01/23/05 and 07/21/06, respectively. The discrepancies in LST estimates vary across the terrain and the temporal granularity of the simulations. Some consistent discrepancies in the results suggest several ways to improve SRAD LST performance as well as the ASTER/MODIS algorithms. Further work should be performed to test these hypotheses using ground measurement data and to demonstrate the efficacy of incorporating spatially distributed factors to improve SRAD model performance.

References

Abrams, M., Hook, S., Ramachandran, B., 2002. ASTER user handbook. Version 2. http://asterweb.jpl.nasa.gov/content/03_data/04_Documents/aster_user_guide_v2.pdf.

Allen, R.G., Pereira, L.S., Raes, D., Smith, M., 1998. Crop Evapotranspiration - Guidelines for Computing Crop Water Requirements. Rome, FAO Irrigation and drainage paper 56. Available from http://www.fao.org/docrep/X0490E/X0490E00.htm.

Davis, M., 1998. Stepping outside the Box: Water in Southern California. Available from. http://www.monolake.org/waterpolicy/outsidebox.htm.

DHI (Danish Hydraulic Institute), 1993. MIKE SHE Water Movement Short Description. Danish Hydraulic Institute, Horsholm: Denmark.

Diak, G.R., Whipple, M.S., 1993. Improvements to models and methods for evaluating the land-surface energy balance and effective roughness using radiosonde reports and satellite-measured skin temperature data. Agriculture and Forestry Meteorology 63, 189–218.

Dubayah, R., 1992. Estimating net solar radiation using Landsat Thematic Mapper and digital elevation data. Water Resource. Research 28, 2469–2484.

Dubayah, R., Rich, P.M., 1995. Topographic solar radiation models for GIS. International Journal of Geographic Information Systems 9, 405–413.

EPA (Environmental Protection Agency), 2000. Storm Water Management Model (SWMM) Version 5.0.009. Washington, DC. Available from http://www.epa.gov/ednnrmrl/models/swmm/index.htm.

Fu, P., Rich, P.M., 2000. The Solar Analyst 1.0 User Manual. Helios Environmental Modeling Institute, KS. Available from. http://www.fs.fed.us/informs/solaranalyst/solar_analyst_users_guide.pdf.

Hook, S., Prata, F., 2001. Land Surface Temperature Measured by ASTER and MODIS—First Results. European Geophysical Society 26th General Assembly, Nice, France, March 25–30 2001. (Abstract).

Hungerford, R.D., Nemani, R.R, Running, S.W., Coughlan, J.C., 1989. MTCLIM: A mountain microclimate simulation model. USDA Forest Service, Research Paper INT-414, Intermountain Research Station, Ogden.

Jacob, F., Petitcolin, F., Schmugge, T., Vermote, E., French, A., Ogawa, K., 2004. Comparison of land surface emissivity and radiometric temperature derived from MODIS and ASTER sensors. Remote Sensing of Environment 90, 137–152.

Julien, P.Y., Saghafian, B., Ogden, F.L., 1995. Raster-based hydrological modeling of spatially-varied surface runoff. Water Resources Bulletin 31, 523–536.

Justice, C., Vermote, E., Townshend, J., Defries, R., Roy, D., Hall, D., Salomonson, V., Privette, J., Riggs, G., Strahler, A., Lucht, W., Myneni, R., Knyazikhin, Y., Running, S., Nemani, R., Wan, Z., Huete, A., van Leeuwen, W., Wolfe, R., Giglio, L., Muller, J.P., Lewis, P., Barnsley, M., 1998. The MODerate Imaging Spectroradiometer (MODIS): Land remote sensing for global change research. IEEE Transactions on Geoscience and Remote Sensing 36, 1228–1249.

Kang, S., Kim, S., Lee, D., 2002. Spatial and temporal patterns of solar radiation based on topography and air temperature. Canadian Journal of Forest Research 32, 487–497.

Krcho, J., 1990. Morphometric analysis and digital models of georelief. VEDA, Bratislava (in Slovak).

Loughhead, A.N., 1994, Environmental modelling for the assessment of property and district plans: a case study in the south-west slopes of New South Wales. HBSc. thesis, Department of Geography, Australian National University, Canberra.

Mannstein, H., 1987. Surface energy budget, surface temperature and thermal inertia. In: Vaughan, R.A., Reidel, D. (Eds.), Remote Sensing Applications in Meteorology and Climatology. NATOASI Series C: Mathematical and Physical Sciences, 201. Reidel, Dordrecht, pp. 391–410.

McKenney, D.W., Mackey, B.G., Zavitz, B.L., 1999. Calibration and sensitivity analysis of a spatially-distributed solar radiation model. International Journal of Geographical Information Science 13 (1), 49–65.

Moore, I.D., Norton, T.W., Williams, J.E., 1993. Modelling environmental heterogeneity in forested landscapes. Journal of Hydrology 150, 717–747.

Mullen, I.C., 1995. Environmental process and landscape pattern: rainforests of the south coast of New South Wales. HBSc. thesis, Department of Geography, Australian National University: Canberra.

NOAA, 2006. Climate of Los Angeles. http://www.wrh.noaa.gov/lox/climate/climate_intro.php.

NRCS (Natural Resources Conservation Service), 1986. Urban Hydrology for Small Watersheds. Technical Release No. 55. USDA, Washington, DC. Available from. http://www.wcc.nrcs.usda.gov/hydro/hydro-tools-models-tr55.html.

Park, S., Feddema, J.J., Egbert, S.L., 2005. MODIS land surface temperature composite data and their relationships with climatic water budget factors in the central Great Plains. International Journal of Remote Sensing 26 (6), 1127–1144.

Price, J.C., 1982. On the use of satellite data to infer surface fluxes at meteorological scales. Journal of Applied Meteorology 21, 1111–1122.

Richardson, K.A., 2003. On the limits of bottom-up computer simulation: Towards a nonlinear modeling culture. In: Sprague, R.H. Jr. (Ed.), Proceedings of the 36th Hawaii International Conference on System Sciences.

Running, S.W., 1991. Computer simulation of regional evapotranspiration by integrating landscape biophysical attributes with satellite data. In: Schmugge, T.J., Andre, J. (Eds.), Land Surface Evaporation: Measurement and parameterization. Springer, London, pp. 359–369.

Running, S.W., Thornton, P.E., 1996. Generating daily surfaces of temperature and precipitation over complex topography. In: Goodchild, M., Steyart, L.T., Parks, B.O. (Eds.), GIS and Environmental Modeling: Progress and Research Issues. GIS World Books, Fort Collins, USA, p. 93.

Running, S.W., Nemani, R.R., Hungerford, R.D., 1987. Extrapolation of synoptic meteorological data in mountainous terrain and its use for simulating forest evapotranspiration and photosynthesis. Canadian Journal of Forest Research 17, 472–483.

Scharmer, K., Greif, J. (Eds.), 2000. The European Solar Radiation Atlas. Database and Exploitation Software, Vol. 2. Les Presses de l' École des Mines, Paris.

Schmugge, T.J., Schmidt, G.M., 1998. Surface temperature observations from AVHRR in FIFE. Journal of the Atmospheric Sciences 55, 1239–1246.

Schoorl, J.M., Sonneveld, M.P.W., Veldkamp, A., 2000. Three-dimensional landscape process modelling: The effect of DEM resolution. Earth Surface Processes and Landforms 25, 1025–1034.

Sellers, P.J., Hall, F.G., Asrar, G., Strebel, D.E., Murphy, R.E., 1988. The first ISLSCP Field Experiment (FIFE). Bulletin of the American Meteorology Society 69, 22–27.

Skahill, B.E., Johnson, L.E., 2000. F2D-a kinematic distributed watershed rainfall-runoff model. NOAA Technical Memorandum OAR FSL-24. Forecast Systems Laboratory, Boulder, CO, 28 pp.

Snyder, W., Wan, Z., Zhang, Y., Feng, Y.Z., 1997. Requirements for Satellite Land Surface Temperature Validation Using a Silt Playa. Remote Sensing of Environment 61, 279–289.

Sun, L., Chen, L., Liu, Q., Liu, Q., Song, A., 2004. Analysis on uncertainty in the MODIS retreived land surface temperature using field measuremnts and high resolution images. The Institute of Electrical and Electronics Engineers IEEE, 2083–2086.

Terjung, W.H., Kickert, R.N., Kochevar, R.J., Mrowka, J.P., Ojo, S.O., Potter, G.L., Tuller, S.E., 1969. The annual march of the topoclimatic spatial patterns of net radiation in Southern California. Theoretical and Applied Climatology 17, 21–50.

Thornton, P.E., Running, S.W., White, M.A., 1997. Generating surfaces of daily meteorology variables over large regions of complex terrain. Journal of Hydrology 190, 214–251.

Thornton, P.E., Hasenauer, H., White, M.A., 2000. Simultaneous estimation of daily solar radiation and humidity from observed temperature and precipitation: An application over complex terrain in Austria. Agricultural and Forest Meteorology 104, 255–271.

USACE-HEC(U.S. Army Corps of Engineers Hydrologic Engineering Center), 1998. HEC-HMS Hydrologic Modeling System user's manual. USACE-HEC, Davis, CA.

Wan, Z., Dozier, J., 1996. A generalized split-window algorithm for retrieving land-surface temperature from space. IEEE Transaction Geoscience and Remote Sensing 34, 892–905.

Wan, Z., Zhang, Y., Zhang, Q., Li, Z., 2002. Validation of the land-surface temperature products retrieved from Terra MODIS data. Remote Sensing of Environment 83, 163–180.

Wan, Z., Zhang, Y., Zhang, Q., 2004. Quality assessment and validation of the MODIS global land surface temperature. International Journal of Remote Sensing 25, 261–274.

Wang, K., Zhou, X., Liu, J., Sparrow, M., 2005. Estimating surface solar radiation over complex terrain using moderate-resolution satellite sensor data. International Journal of Remote Sensing 26 (1), 47–58.

Wilson, J.P., Gallant, J.C. (Eds.), 2000a. Terrain Analysis: Principles and Applications. John Wiley & Sons, New York.

Wilson, J.P., Gallant, J.C., 2000b. Secondary topographic attributes. In: Wilson, J.P., Gallant, J.C. (Eds.), Terrain Analysis: Principles and Applications. John Wiley & Sons, New York, pp. 51–85.

Yang, H., Yang, Z., 2006. A modified land surface temperature split window retrieval algorithm and its applications over China. Global and Planetary Change 52, 207–215.